

# Orally Fast-Disintegrating Resveratrol/Cyclodextrin Nanofibrous Films as a Potential Antioxidant Dietary Supplement

Asli Celebioglu,<sup>\*,†</sup> Deniz Tekant,<sup>†</sup> Mehmet Emin Kilic, Engin Durgun, and Tamer Uyar<sup>\*</sup>Cite This: *ACS Food Sci. Technol.* 2022, 2, 568–580

Read Online

ACCESS |



Metrics &amp; More



Article Recommendations



Supporting Information

**ABSTRACT:** Encapsulation of dietary supplements into electrospun cyclodextrin (CD) inclusion complex (IC) nanofibers can pave the way for the development of novel delivery systems with orally fast-disintegrating properties. Here, resveratrol/CD-IC nanofibrous films were fabricated using the electrospinning technique. Resveratrol is a well-known bioactive agent with its antioxidant potential, and it is commonly used in the formulation of dietary supplements. Here, the hydroxypropylated (HP-)  $\beta$ CD and  $\gamma$ CD were used for both encapsulation of resveratrol and the electrospinning of free-standing nanofibrous films. SEM imaging confirmed the uniform fibrous morphology of electrospun films. The encapsulation and amorphization of resveratrol by inclusion complexation were verified using various techniques including FTIR,  $^1\text{H}$  NMR, XRD, DSC, TGA, and computational modeling. Besides the results of all these techniques, phase solubility studies also revealed the more favorable complex formation of resveratrol with HP $\beta$ CD compared to HP $\gamma$ CD. Nanofibrous films were obtained having  $\sim$ 100% loading efficiency without a loss during the process. The amorphous distribution of resveratrol and the unique properties of nanofibers ensured the fast disintegration of nanofibrous films in the saliva simulation. The enhanced solubility of resveratrol also ensured an improved antioxidant property. The polymeric resveratrol/pullulan nanofibrous film was also formed as a control sample. CD-IC nanofibrous films showed faster disintegration/dissolution, higher/faster release profile, and significantly better antioxidant potential compared to resveratrol/pullulan-based samples.

**KEYWORDS:** *resveratrol, cyclodextrin, electrospinning, nanofibers, orally fast disintegrating, dietary supplement, antioxidant, fast release, enhanced solubility*

## 1. INTRODUCTION

Bioactive compounds including antioxidants, vitamins, aromas, essential oils, and so forth hold important properties having the potential to promote human health. Therefore, they have aroused growing interest in the food and pharmaceutical industries and have been widely used in the formulation of dietary supplements. However, the drawbacks of poor water solubility, low bioavailability, and low stability against light, heat, and oxygen create challenges during their processing, storage, and consumption. Hence, these bioactive compounds are being encapsulated into a proper carrier system in order to ensure enhanced water solubility, bioavailability, and a longer shelf-life.<sup>1</sup> As encapsulation techniques, freeze-drying, spray-drying, co-precipitation, emulsion, or extrusion can come into prominence.<sup>1</sup> On the other hand, the electrohydrodynamic approach of electrospinning has recently appeared to be a promising alternative method for the encapsulation of bioactive compounds in the matrices of nanofibers having submicron diameters.<sup>2</sup> Electrospun films combined with bioactive compounds display a huge potential to be used in food-based applications owing to their free-standing, flexible, and highly porous structure.<sup>3,4</sup> The electrospun films based on biopolymers having insoluble nature in water can be effectively used for food packaging purposes when they are incorporated with bioactive compounds.<sup>5</sup> In other respects, the use of hydrophilic and edible polymers for the generation of functional electrospun films can enable to obtain fast

disintegrating delivery systems which can freely disintegrate upon contact with aqueous medium.<sup>6,7</sup> In our latest reports, we demonstrated that the fast-disintegrating delivery system can be also obtained from the electrospun nanofibrous films of cyclodextrin (CD) inclusion complexes of different bioactive compounds including antioxidants<sup>8–10</sup> and vitamins.<sup>9</sup>

As a type of oligosaccharide, CDs have drawn great attention of worldwide market of food and pharmaceutical industries.<sup>11–13</sup> Since CDs are classified as Generally Recognized as Safe (GRAS) by the US Food and Drug Administration, they are being used in the formulation of drugs and nutrition-based products.<sup>14</sup> These starch-derived molecules can form non-covalent interactions with a variety of molecules, and this makes them the main source of interest as an encapsulation agent. As a result of inclusion complexation with CD, the aqueous solubility, bioavailability, and stability of bioactive compounds or drug molecules can be improved markedly.<sup>12,15</sup> In addition, different release profiles such as fast, controlled and/or sustained, masking of unpleasant taste/odor and longer shelf-life can be provided by this approach.<sup>15,16</sup>

**Received:** December 15, 2021

**Revised:** February 21, 2022

**Accepted:** February 23, 2022

**Published:** March 4, 2022



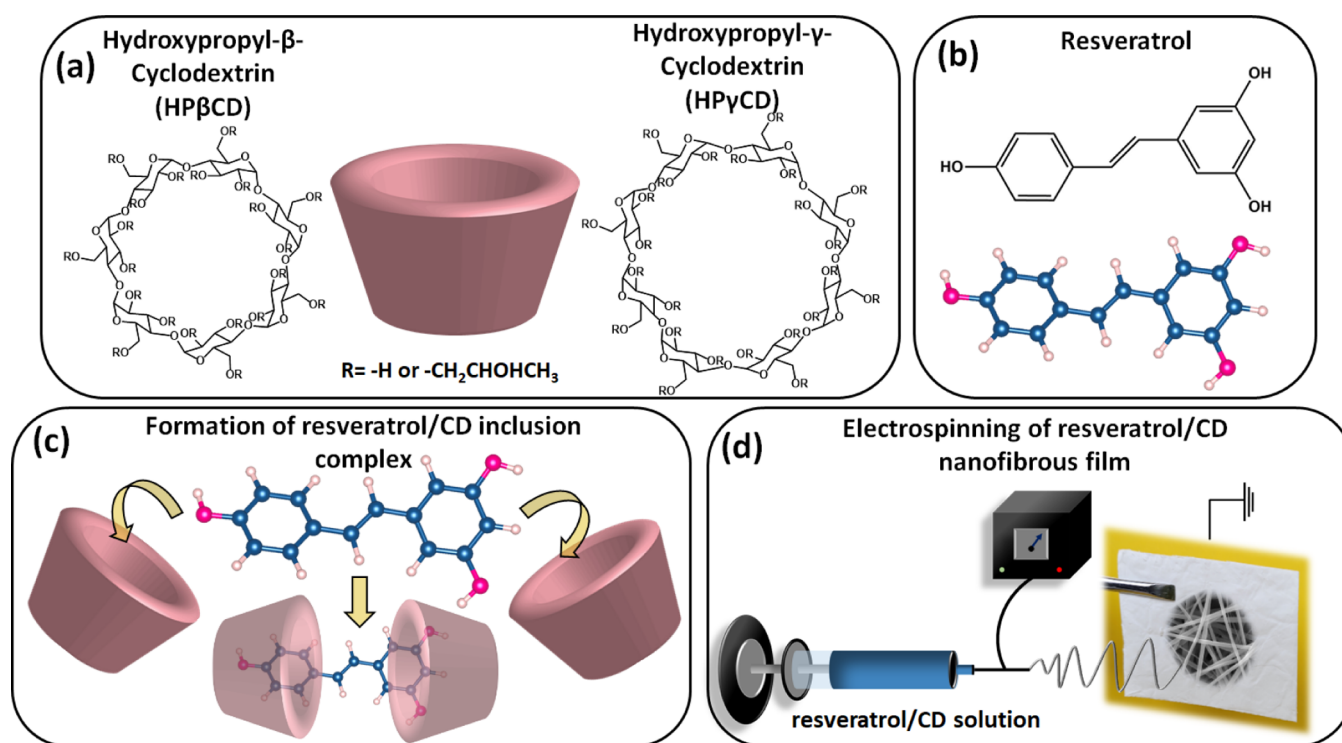


**Figure 1.** Main concept of the study. Chemical structure of (a) HPβCD and HPγCD and (b) resveratrol. (c) Schematic representation of inclusion complex formation between resveratrol and CDs and (d) electrospinning of resveratrol/CD nanofibrous films.

Resveratrol is a nonflavonoid polyphenolic compound from the stilbene family and it is generally found in different types of fruits and vegetables and especially in grape skins.<sup>17</sup> Resveratrol is known to possess antioxidant, anti-inflammatory, antibacterial, and anticarcinogenic properties.<sup>18,19</sup> Therefore, it displays great potential for the treatment of various diseases including cancer, diabetes, obesity, arthritis, cardiovascular disorders, and so forth.<sup>18,19</sup> Despite all its benefits, the poor water solubility, low bioavailability, and low stability limit the application potential of this bioactive compound.<sup>20</sup> To overcome these drawbacks, emulsions, liposomes, biopolymeric particles, and CD inclusion complexes were utilized as different encapsulation approaches.<sup>21</sup> The inclusion complexation with CD particularly showed the increased water solubility of resveratrol for different types of CDs.<sup>20</sup> Nanotechnology-based formulations have also been reported for improving the bioactivity of resveratrol molecules.<sup>22</sup> There are several studies in the literature in which the electrospinning technique was employed for the encapsulation of resveratrol in the polymeric nanofibrous films, as well.<sup>23–26</sup> However, there has been no study reported that is related to the electrospinning of polymer-free nanofibrous films from the resveratrol/CD inclusion complexes for the development of orally fast-disintegrating dietary supplement. Orally disintegrating tablets (ODTs) have already been followed with great interest over the last decades in the pharmaceutical industry.<sup>27</sup> ODT formulations can provide an extra convenience for the users compared to conventional tablets because they can disintegrate in the oral cavity instantly upon contact with the saliva. Here, additional liquid or chewing activity is not essential during their administration, so ODTs are especially useful for ones who have difficulties in chewing and swallowing process or having problem of vomiting.<sup>27,28</sup> In addition to ease of implementation, the water solubility, bioavailability, and

delivery of poorly soluble compounds can be improved by ODT.<sup>27,28</sup> As mentioned previously, resveratrol shows poor bioavailability and this is because of phase II and presystemic metabolism of this bioactive compound throughout the gastrointestinal tract.<sup>29</sup> The very recent studies showed that the transmucosal pathway can be an alternative administration route to enhance the permeation of resveratrol across the tissues.<sup>29–31</sup> Since oral mucosa is highly vascularized, it enables the direct absorption of compounds into the systemic circulation, so the first-pass hepatic metabolism is eliminated by bypassing the gastrointestinal tract.<sup>32</sup> Herein, orally disintegrating delivery systems can be a solution to profit from therapeutic potential of resveratrol by applying the alternative route of oral mucosa.

In our very recent studies, we have shown that the nanofibrous films of drug/CD inclusion complexes might have potential to be used for fast-disintegrating delivery systems as an alternative to the ODT formulations.<sup>33–36</sup> Therefore, the fast disintegrating nanofibrous films of resveratrol might be a promising alternative to the commercially available tablet formulations. For that purpose, we achieved to produce electrospun nanofibrous films of resveratrol/CD inclusion complexes in aqueous medium without using an additional polymeric carrier matrix or unfavorable/toxic chemicals (Figure 1). Here, the highly water-soluble and hydroxypropylated derivatives of CD, hydroxypropyl-β-cyclodextrin (HPβCD) and hydroxypropyl-γ-cyclodextrin (HPγCD), were chosen and resveratrol/pullulan nanofibrous films were produced as a control sample, as well. The structural analyses, dissolution/disintegration, release, and antioxidant profiles of samples were evaluated further.

## 2. MATERIALS AND METHODS

**2.1. Materials.** Hydroxypropyl- $\beta$ -cyclodextrin (HP $\beta$ CD) (Cavasol W7 HP, DS:  $\sim$ 0.9) and hydroxypropyl- $\gamma$ -cyclodextrin (HP $\gamma$ CD) (Cavasol W8 HP Pharma, DS:  $\sim$ 0.6) are kind gift of Wacker Chemie AG (USA) for our scientific research. The as-received pullulan ( $M_w$  300,000 g/mol, TCI America), resveratrol (99%, TCI America), 2,2-diphenyl-1-picrylhydrazyl (DPPH,  $\geq$ 97%, TCI America), methanol ( $\geq$ 99.8% (GC), Sigma-Aldrich), dimethyl sulfoxide (DMSO,  $>$ 99.9%, Sigma-Aldrich), sodium chloride (NaCl,  $>$ 99%, Sigma-Aldrich), *o*-phosphoric acid (85% (HPLC), potassium phosphate monobasic (KH<sub>2</sub>PO<sub>4</sub>,  $\geq$ 99.0%, Fisher Chemical), sodium phosphate dibasic heptahydrate (Na<sub>2</sub>HPO<sub>4</sub>, 98.0–102.0%, Fisher Chemical), Fisher Chemical), phosphate-buffered saline (PBS) tablets (pH 7.4, Sigma-Aldrich), and deuterated dimethylsulfoxide (DMSO-*d*<sub>6</sub>, 99.8%, Cambridge Isotope) were provided commercially. The high-quality distilled water was obtained using a Millipore Milli-Q ultrapure water system (Millipore, USA).

**2.2. Phase Solubility Study.** The phase solubility profile of resveratrol/CD was determined as reported previously.<sup>37</sup> Here, excess amount of resveratrol ( $\sim$ 2.8 mM) was mixed with the increasing concentration of CD from 0 to 6 mM in 5 mL of water. After shaking on an incubator shaker (450 rpm, shielded from light, room temperature) for 24 h, each suspension was filtered with PTFE filter (0.45  $\mu$ m). Then, filtered aliquots were measured using UV–vis spectroscopy (317 nm) (PerkinElmer, Lambda 35, USA) and their absorbance intensity was converted to concentration (mM) by the calibration curve of resveratrol taken in water ( $R^2 \geq 0.99$ ). The phase solubility diagrams of HP $\beta$ CD and HP $\gamma$ CD were plotted using the mean values  $\pm$  standard deviations of triplicate measurements. The equation below was used to calculate the binding constants ( $K_s$ ).

$$K_s = \text{slope}/S_0(1 - \text{slope}) \quad (1)$$

where  $S_0$  is the intrinsic solubility of resveratrol ( $\sim$ 0.17 mM).

**2.3. Computational Methodology.** First-principles computational methods based on density functional theory (DFT)<sup>38,39</sup> implemented in VASP<sup>40</sup> were employed to study the interaction of resveratrol molecules with CDs. Generalized gradient approximation (GGA-PBE) was utilized for the exchange–correlation functional.<sup>41</sup> The van der Waals interactions were taken into account using the Grimme method (DFT-D2).<sup>42</sup> The element potentials were identified by projector augmented-wave (PAW) potentials<sup>43</sup> with 520 eV kinetic energy cutoff. All the structures were optimized by the conjugate gradient method by setting the energy and force criteria to  $10^{-5}$  eV and  $10^{-2}$  eV/Å. The interaction between the structures and water was examined using the implicit solvation model where continuum dielectric description was implemented.<sup>44</sup>

**2.4. Electrospinning.** The clear solutions of CD and pullulan were, respectively, prepared by the solid concentration of 180% (w/v) and 20% (w/v) in water. Resveratrol powder was subsequently added to CD and pullulan solutions to provide  $\sim$ 7% resveratrol content (w/w, in proportion to total sample amount). This resveratrol amount corresponds to the molar ratio of 1:2 (guest/CD) in the case of resveratrol/HP $\beta$ CD and resveratrol/HP $\gamma$ CD systems and these solutions were stirred overnight to ensure the inclusion complex formation between resveratrol and CD molecules. The control samples of pristine CD and pullulan solutions were prepared having solid concentrations of 200 and 20% (w/v), respectively. The solution properties of viscosity and electrical conductivity were verified for each system using a rheometer (AR 2000 rheometer, TA Instruments, USA) [cone/plate spindle (20 mm diameter and 4° cone angle), shear rate range: 0.01–1000 s<sup>-1</sup> (21 °C)] and conductivity meter (FiveEasy, Mettler Toledo, USA), respectively. The electrospinning process was performed using the configurable electrospinning equipment (Spingenix, model: SG100, Palo Alto, USA). The resveratrol/HP $\beta$ CD, resveratrol/HP $\gamma$ CD, and resveratrol/pullulan aqueous systems were separately loaded into plastic syringes (1 mL) that were fitted with metallic nozzles (23 G). The electrospinning parameters of flow rate, high voltage, and nozzle-to-collector distance were applied as 0.5 mL/h, 15 kV, and 15 cm, respectively, to

deposit electrospun nanofibrous films on the grounded stationary metal collector. The temperature and relative humidity were observed to be 45% and 21 °C, respectively, throughout the electrospinning of nanofibers. It is noteworthy to point out that resveratrol/HP $\beta$ CD and resveratrol/HP $\gamma$ CD aqueous systems had been first prepared with 1:1 (guest/CD) molar ratio; however, the high heterogeneity of these systems precluded the generation of nanofibrous films efficiently.

**2.5. Structural Characterizations.** The morphology of electrospun HP $\beta$ CD, HP $\gamma$ CD, pullulan, resveratrol/HP $\beta$ CD, resveratrol/HP $\gamma$ CD, and resveratrol/pullulan nanofibers was examined using scanning electron microscopy (SEM, Tescan MIRA3, Czech Republic). For the measurements, the samples were fixed on the SEM stubs and coated with a thin Au/Pd layer to reduce the charging problem. SEM imaging was performed under high vacuum with a working distance of 10 mm by applying an accelerating voltage of 10 kV. The average diameter (AD) (mean values  $\pm$  standard deviations) of samples ( $\sim$ 100 fibers) was calculated using ImageJ software. The crystalline and the amorphous structures of resveratrol powder, HP $\beta$ CD, HP $\gamma$ CD, pullulan, resveratrol/HP $\beta$ CD, resveratrol/HP $\gamma$ CD and resveratrol/pullulan nanofibrous films were evaluated using an X-ray diffractometer (Bruker D8 ADVANCE ECO, USA) ( $2\theta$  region: 5°–30°; radiation source: Cu K $\alpha$ ; current/voltage: 25 mA/40 kV). The thermal profile of the samples was examined by differential scanning calorimetry (DSC, Q2000, TA Instruments, USA) (temperature range: 0–280 °C; heating rate: 10 °C/min N<sub>2</sub>) and thermogravimetric analysis (TGA, Q500, TA Instruments, USA) (temperature range: 25–600 °C; heating rate: 20 °C/min, N<sub>2</sub>). Additionally, attenuated total reflectance Fourier transform infrared spectrometry (ATR-FTIR, PerkinElmer, USA) was conducted to record the FTIR spectra of the samples (4000–600 cm<sup>-1</sup>; resolution of 4 cm<sup>-1</sup>; 64 scans). A proton nuclear magnetic resonance (<sup>1</sup>H NMR) spectrometer (Bruker AV500 with autosampler, USA) was used to verify the loading of resveratrol and to determine the rough amount of resveratrol in resveratrol/HP $\beta$ CD, resveratrol/HP $\gamma$ CD, and resveratrol/pullulan nanofibrous films (solvent: DMSO-*d*<sub>6</sub>; sample concentration: 40 mg/mL; 16 scan). Mestranova software was used to process <sup>1</sup>H NMR spectra.

**2.6. Loading Efficiency.** To calculate the loading efficiency of samples, a certain amount ( $\sim$ 5 mg) of resveratrol/HP $\beta$ CD, resveratrol/HP $\gamma$ CD, and resveratrol/pullulan nanofibrous films were dissolved in dimethyl sulfoxide (DMSO) (5 mL). Then, UV–vis spectroscopy (326 nm) was used to determine the loaded resveratrol content in the samples (the calibration curve in DMSO;  $R^2 \geq 0.99$ ). The experiments were performed in triplicate. The equation given below was used for the calculation.

$$\text{Loading efficiency (\%)} = C_e/C_i \times 100 \quad (2)$$

where  $C_e$  is the loaded resveratrol concentration and  $C_i$  is the initial resveratrol concentration.

**2.7. Dissolution and Disintegration Test.** The dissolution profile of resveratrol powder, resveratrol/CD nanofibrous films, and resveratrol/pullulan nanofibrous film was examined by adding 5 mL of PBS into the vials. Here,  $\sim$ 15 mg of nanofibrous films and  $\sim$ 1 mg of resveratrol powder [according to the initial resveratrol content of  $\sim$ 7 (w/w)] were used and a video was recorded simultaneously during the test (Video S1). To examine the disintegration profile of samples, artificial saliva (2.38 g of Na<sub>2</sub>HPO<sub>4</sub>, 0.190 g of KH<sub>2</sub>PO<sub>4</sub>, and 8 g of NaCl in 1 L of distilled water; phosphoric acid for pH 6.8) was made to simulate the moist environment of the tongue.<sup>45</sup> Then, the filter paper located into Petri dishes (10 cm) was moistened with this 10 mL of artificial saliva. After the excess artificial saliva was removed from the Petri dishes, nanofibrous webs ( $\sim$ 3 cm  $\times$  4.5 cm) were put onto the filter paper while a video was filmed concurrently (Video S2).

**2.8. In Vitro Release Test.** The time-dependent *in vitro* release test of resveratrol/CD and resveratrol/pullulan nanofibrous films was conducted for the sample concentration of 1 mg/mL in PBS buffer (pH 7.4) at 37 °C. The 0.25 mL of test aliquots was withdrawn, and the same amount of fresh PBS medium (0.25 mL) was added at the predetermined times while the solutions were shaken on the incubator



(200 rpm). Then, UV measurements of these aliquots were performed (317 nm) to assess the released amount of resveratrol from nanofibrous films. The absorbance intensity of each measurement was converted into released % using the calibration curve ( $R^2 \geq 0.99$ ). The release profile (released %) of samples was plotted against time using the triplicate measurement results in mean values  $\pm$  standard deviations. Different kinetic models were used to evaluate the release kinetics and the details are summarized in the [Supporting Information](#).

**2.9. Antioxidant Activity Test.** 2,2-Diphenyl-1-picrylhydrazyl (DPPH) radical scavenging assay was used to evaluate the antioxidant potential of samples. The aqueous solutions of nanofibrous films and the resveratrol powder were prepared with the increasing resveratrol concentration of 13 to 210  $\mu\text{g/mL}$ . Each solution had a different resveratrol concentration and was mixed with the methanolic solution of DPPH (75  $\mu\text{M}$ ) at a volume ratio of 6/1, v/v (DPPH/sample). Then, they were incubated in the dark for 30 min and the DPPH absorption intensity of solutions was measured (517 nm) using UV-vis spectroscopy. The results were given as mean  $\pm$  standard deviation for the triplicate experiments of all samples. The radical inhibition activity of each sample was calculated in terms of % using the equation given below.

$$\text{Inhibition (\%)} = (A_{\text{control}} - A_{\text{sample}}) / A_{\text{control}} \times 100 \quad (3)$$

where  $A_{\text{sample}}$  is the absorbance of sample solution and  $A_{\text{control}}$  is the absorbance of control DPPH solution. The concentration-dependent results also enabled to calculate the 50% inhibition value (IC50), which shows the essential amount of the sample to reduce the absorption intensity of DPPH by 50%.<sup>46</sup>

**2.10. Statistical Analyses.** The statistical analyses were conducted using the one-way/two-way of variance (ANOVA). OriginLab (Origin 2021, USA) was used for all these ANOVA analyses (0.05 level of probability).

### 3. RESULTS AND DISCUSSION

**3.1. Phase Solubility Analysis.** The phase solubility analysis was conducted to examine the effects of increasing HP $\beta$ CD and HP $\gamma$ CD concentrations on the solubility of resveratrol molecules, as depicted in [Figure 2](#). The linear

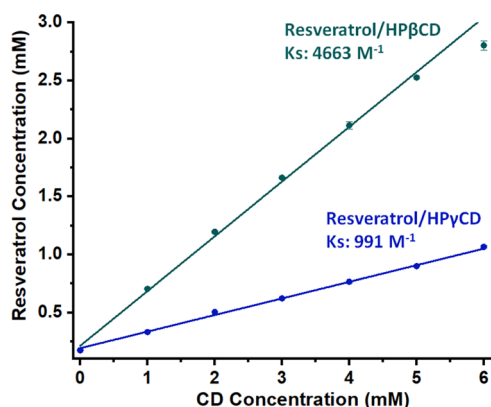


**Figure 2.** Phase solubility study. Phase solubility diagram of resveratrol/HP $\beta$ CD and resveratrol/HP $\gamma$ CD systems.

relationship between resveratrol and modified CD concentrations observed in the diagram points to the  $A_L$ -type profile. As stated by Higuchi and Connors, the phase solubility diagram having  $A_L$ -type profiles suggests the development of inclusion complexes having a 1:1 molar ratio (guest/CD).<sup>37</sup> While the solubility of resveratrol without CD was denoted as  $\sim 0.17$  mM, it was able to achieve  $\sim 16.3$  times higher solubility with HP $\beta$ CD inclusion complexation. On the other hand,

resveratrol molecules were able to achieve  $\sim 6.2$  times higher solubility in the presence of HP $\gamma$ CD. As seen in [Figure 2](#), the binding constants ( $K_s$ ) were, respectively, calculated as 4663 and 991  $\text{M}^{-1}$  for HP $\beta$ CD and HP $\gamma$ CD systems for the noted experimental conditions. The statistical analysis also showed that there is a significant difference between CDs ( $p < 0.05$ ). The distinct variation between the resveratrol/HP $\beta$ CD and resveratrol/HP $\gamma$ CD system might be due to HP $\beta$ CD providing a better cavity size matching compared to HP $\gamma$ CD.<sup>47</sup> This led to a much larger  $K_s$  value and hence, more solubility for the resveratrol/HP $\gamma$ CD inclusion complex system compared to the resveratrol/HP $\beta$ CD one. The  $K_s$  value for the resveratrol/HP $\gamma$ CD system could not be found from the previous reports in the literature. On the other hand, in other related studies in which the phase solubility test was performed for HP $\beta$ CD, the  $A_L$ -type diagrams were also obtained with a similar range of  $K_s$  values such as 6778,<sup>48</sup> 5988,<sup>49</sup> and 6960  $\text{M}^{-1}$ .<sup>50</sup> The slight differences between  $K_s$  might be due to different substitution degrees of HP $\beta$ CD used in the studies which can lead to different binding strengths between CD and guest molecules.<sup>51</sup>

**3.2. Computational Modeling Analysis.** To understand the complexation between resveratrol molecules and HP $\beta$ CD and HP $\gamma$ CD, computational modeling studies were performed. Initially, the resveratrol and CDs were separately optimized in vacuum and water. Afterward, the interaction of resveratrol with both CDs was examined by considering the orientation of the molecule [head (H)–tail (T)] and rims of the CDs [wide (B)–narrow (A)]. The variation of energy with respect to the location of resveratrol and CDs revealed that IC can be formed for both HP $\beta$ CD and HP $\gamma$ CD without providing activation energy. CD-IC configurations for 1:1 and 1:2 stoichiometries are shown in [Figure 3](#). For 1:1 stoichiometry, T- and H-orientations were preferred for HP $\beta$ CD and HP $\gamma$ CD, respectively. As width of HP $\gamma$ CD is larger than HP $\beta$ CD, resveratrol moved toward the HP arms to strengthen the interaction. For 1:2 stoichiometry, while the tail of resveratrol was inside the CD, the head part interacted with the wide rim for both of the cases. Similar configurations were also obtained when calculations were repeated in water. The complexation energy ( $E_{\text{CE}}$ ) with and without solvent can be estimated as

$$E_{\text{CE}} = n \times E[\text{CD}] + E[\text{resveratrol}] - E[\text{CD-IC}] \quad (4)$$

where  $E[\text{CD}]$ ,  $E[\text{resveratrol}]$ , and  $E[\text{CD-IC}]$  are the total energy (in vacuum or in water) of HP $\beta$ CD or HP $\gamma$ CD, resveratrol, and CD-IC, respectively, and  $n$  is equal to 1 (2) for 1:1 (1:2) stoichiometry. The obtained values are summarized in [Table 1](#) and they pointed out that stable resveratrol:HP $\beta$ CD-IC and resveratrol:HP $\gamma$ CD-IC configurations can be formed within 1:1 and 1:2 stoichiometries. It is noticed that even the inclusion in water did not significantly alter the IC configurations, the strength of interaction between resveratrol and CD reduced. The decrease in  $E_{\text{CE}}$  can be related to the interaction of phenolic hydroxyl groups with water.<sup>52</sup> Our results also revealed that the poor solubility of resveratrol in water can be intensely improved by complexation. This effect can be quantified by calculating the solvation energy ( $E_{\text{SE}}$ )

$$E_{\text{SE}} = E^{\text{water}}[\text{CD-IC}] - E^{\text{vacuum}}[\text{CD-IC}] \quad (5)$$

$E^{\text{water}}[\text{CD-IC}]$  and  $E^{\text{vacuum}}[\text{CD-IC}]$  are the total energy of resveratrol:HP $\beta$ CD-IC and resveratrol:HP $\gamma$ CD-IC in water and vacuum, respectively, as listed in [Table 1](#). While  $E_{\text{SE}}$  of resveratrol was calculated as  $-69.04$  kJ/mol, it increases up to

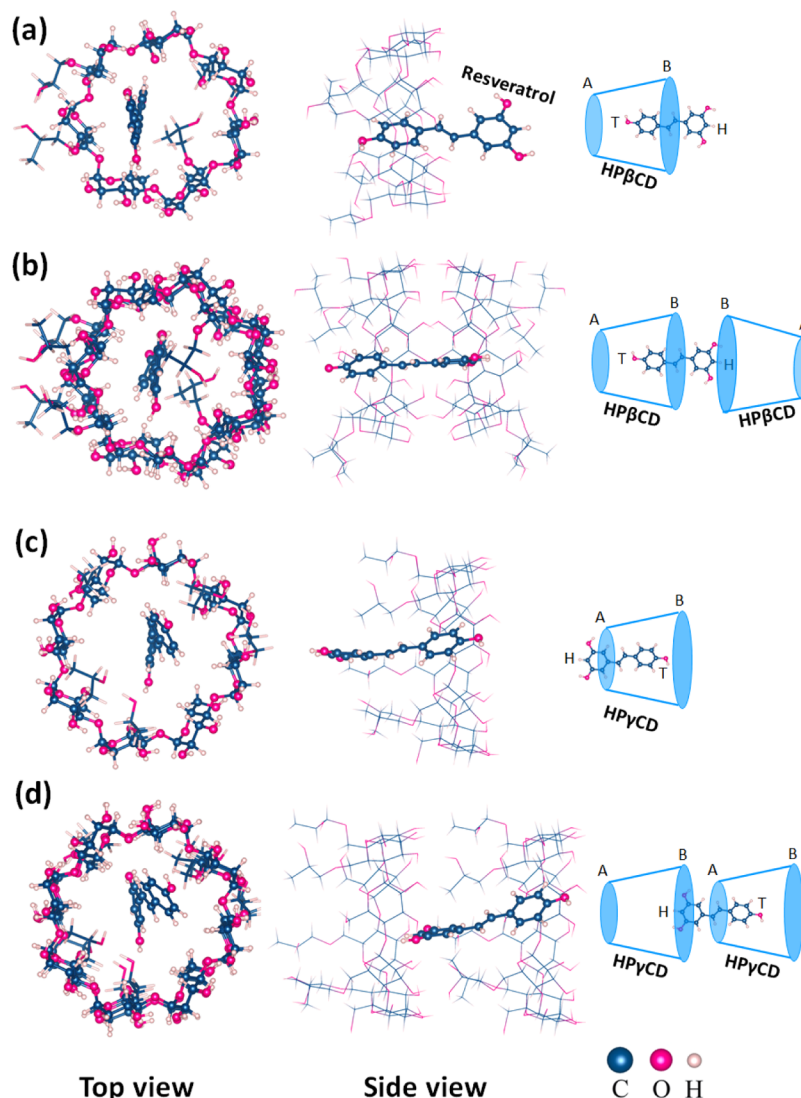


**Figure 3.** Modeling study showing interaction between CDs and resveratrol. The top and side view of resveratrol:HP $\beta$ CD-IC for (a) 1:1 and (b) 1:2 and resveratrol:HP $\gamma$ CD-IC for (c) 1:1 and (d) 1:2 stoichiometry. The orientation of resveratrol (head-H and tail-T) and CDs (narrow rim-A and wide rim-B) is shown.

**Table 1.** Complexation ( $E_{CE}$ ) and Solvation Energies ( $E_{SE}$ ) of Resveratrol/HP $\beta$ CD and Resveratrol/HP $\gamma$ CD Systems for Different Orientations in 1:1 and 1:2 Stoichiometry (Molar Ratio)

guest/host	molar ratio	orientation <sup>a</sup>	$E_{CE}^{\text{Vacuum}}$ kJ/mol	$E_{CE}^{\text{Water}}$ kJ/mol	$E_{SE}$ kJ/mol
resveratrol/HP $\beta$ CD	1:1	H-AB	51.80		
resveratrol/HP $\beta$ CD	1:1	T-AB	68.53	60.29	−329.74
resveratrol/HP $\beta$ CD	1:2	T-ABAB	128.61		
resveratrol/HP $\beta$ CD	1:2	T-ABBA	328.61	154.35	−445.80
resveratrol/HP $\gamma$ CD	1:1	H-AB	107.32	81.80	−359.03
resveratrol/HP $\gamma$ CD	1:1	T-AB	54.68		
resveratrol/HP $\gamma$ CD	1:2	H-ABAB	236.02	144.35	−628.90
resveratrol/HP $\gamma$ CD	1:2	H-ABBA	178.24		

<sup>a</sup>Orientation of resveratrol: head-H and tail-T; orientation of CDs: narrow rim-A and wide rim-B.

−445.80 and −628.90 kJ/mol for resveratrol:HP $\beta$ CD-IC (1:2) and resveratrol:HP $\gamma$ CD-IC (1:2), respectively. This significant increase in  $E_{SE}$  indicated the enhancement in solubility. It is also obvious from Table 1 that the  $E_{CE}^{\text{vacuum}}$  and  $E_{CE}^{\text{water}}$  values were found higher in the case of 1:2 stoichiometry for both CD types compared to 1:1 stoichiometry suggesting our findings of

the electrospinning process which will be discussed in the following section.

**3.3. Morphology of Nanofibrous Films.** In this study, the aqueous systems of resveratrol/CD were initially prepared having a 1:1 molar ratio (guest/CD). However, the heterogeneity of the solutions did not enable to obtain polymer-free and free-standing nanofibers from these systems.

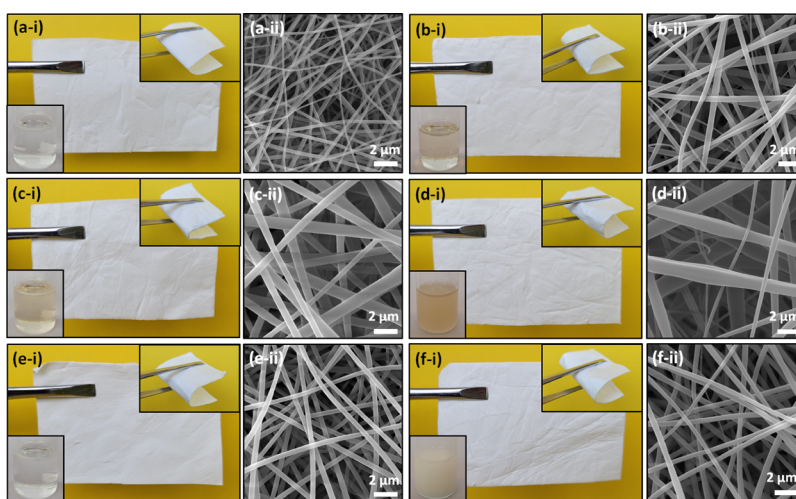


**Figure 4.** Visual examination and morphological analyses. (i) Photographs of electrospinning solutions and the ultimate nanofibrous films (NF) and (ii) SEM images of (a) HP $\beta$ CD NF, (b) resveratrol/HP $\beta$ CD NF, (c) HP $\gamma$ CD NF (d) resveratrol/HP $\gamma$ CD NF, (e) pullulan NF, and (f) resveratrol/pullulan NF.

This finding is not coherent with the phase solubility result in which the A<sub>L</sub>-type diagram was detected showing the existence of a 1:1 molar ratio between CD and guest molecules. However, the electrospinning system is significantly concentrated (180% CD, w/v) compared to the phase solubility one (0.9% CD, w/v). This might be the reason to observe the heterogeneous structure for the 1:1 molar ratio-based electrospinning solutions which may limit the efficient stirring of the system to attain 1:1 complexation. On the other hand, the 1:2 molar ratio was optimized to generate nanofibers from both resveratrol/CD systems which was also supported with the computational modeling calculations. Here, the pristine systems of pullulan and CDs had clear solutions that were able to produce free-standing nanofibers with the electrospinning technique (Figure 4-i). The resveratrol/HP $\beta$ CD solution was also suggesting the complete complexation between HP $\beta$ CD and resveratrol, while the resveratrol/HP $\gamma$ CD and resveratrol/pullulan solutions were turbid showing the existence of uncomplexed resveratrol content in these systems (Figure 4-i). Nevertheless, free-standing and flexible nanofibrous films that can be folded without damage were obtained for all systems (Figure 4). As displayed in Figure 4, the morphologies of each system were examined using the SEM technique which confirmed the homogeneous and defect-free nanofiber formation for all samples. Additionally, CD, pullulan, and resveratrol concentrations along with the solution viscosity, conductivity, and nanofiber's AD are summarized in Table S1 for each system. In previous studies, it was shown that the viscosity and conductivity properties of solutions are the most prominent elements influencing the morphology of the obtained nanofibers.<sup>4,53</sup> As seen in Table S1, the systems containing HP $\gamma$ CD have higher viscosities and lower conductivities compared to the systems containing HP $\beta$ CD. This indicates that HP $\gamma$ CD solutions were less exposed to stretching during the electrospinning process and hence were able to produce thicker fibers (Table S1). We can confirm this by comparing the ADs of the nanofibers: while the resveratrol/HP $\gamma$ CD system was able to produce nanofibers with an AD of  $760 \pm 370$  nm, the resveratrol/HP $\beta$ CD system was able to produce fibers with  $400 \pm 160$  nm thickness. On the other hand, we also observe that pullulan had a much lower viscosity;

thus, we can expect thinner fibers ( $385 \pm 70$  nm). However, it is approximately in the same range of resveratrol/HP $\beta$ CD nanofibers. This could point to another solution property affecting the diameter of fibers such as the surface tension of solutions since it is a polymer-based system compared to the other CD-based solutions.<sup>4</sup> For all systems, the addition of resveratrol to the pristine CD and pullulan slightly increased the conductivity values of the solutions, while a significant change for the viscosity values was not detected (Table S1). Depending on that, we could not find a steady trend in the AD of samples. The results of statistical calculations showed that the diameter of HP $\beta$ CD nanofibers is significantly different from all others ( $p < 0.05$ ). On the other hand, there is no significant differences between HP $\gamma$ CD and resveratrol/HP $\beta$ CD; resveratrol/HP $\beta$ CD and pullulan; and resveratrol/HP $\beta$ CD and resveratrol/pullulan nanofibers ( $p > 0.05$ ).

**3.4. Structural Characterization.** To analyze the crystalline pattern of the samples, powder X-ray diffraction (XRD) was utilized, and the measurement results are displayed in Figure 5. Resveratrol has a crystalline structure, and this can be seen in the graph by the intense and sharp diffraction peaks

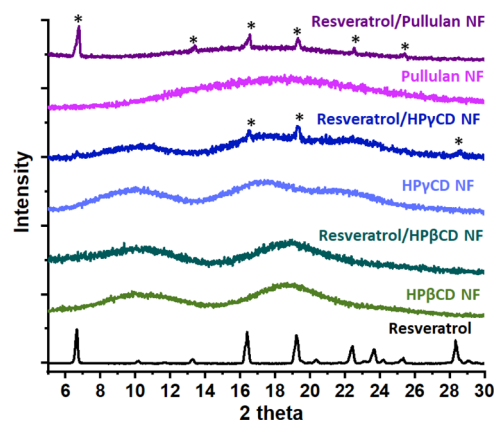


**Figure 5.** Examination of crystal profile of samples. XRD patterns of resveratrol powder, HP $\beta$ CD NF, resveratrol/HP $\beta$ CD NF, HP $\gamma$ CD NF, resveratrol/HP $\gamma$ CD NF, pullulan NF, and resveratrol/pullulan NF.



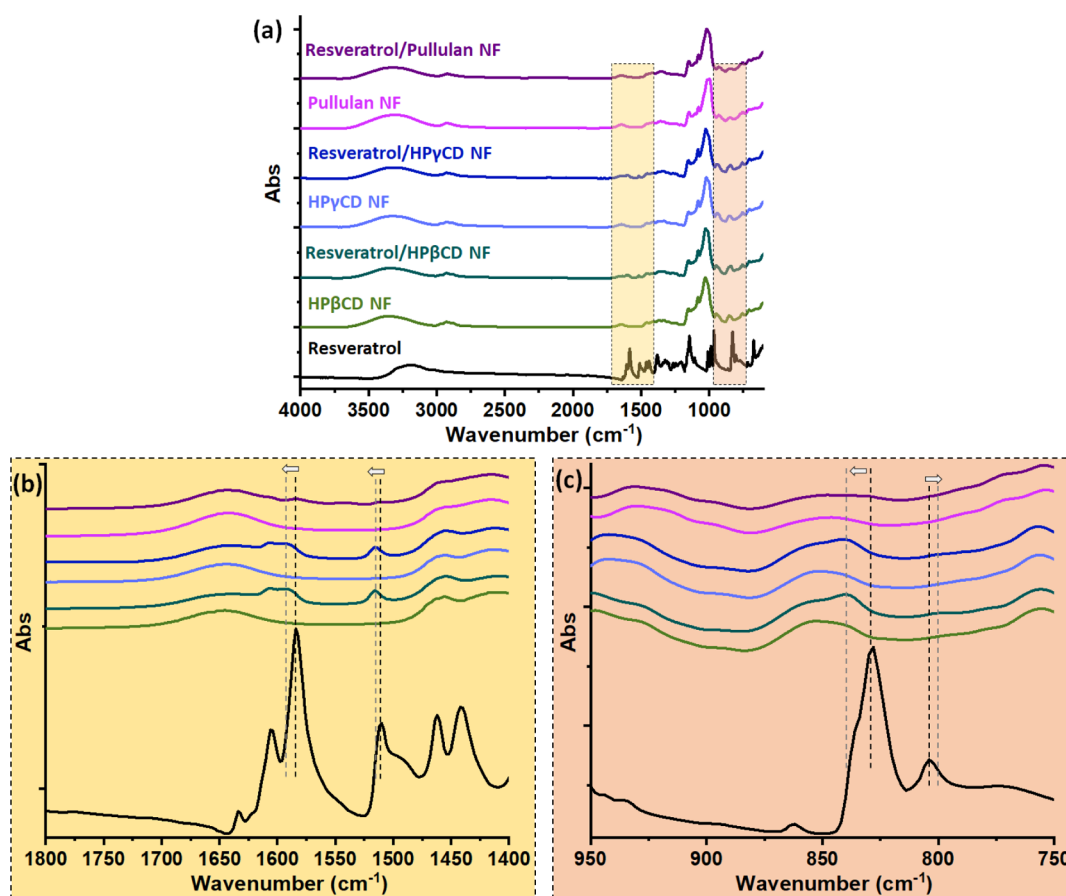


**Figure 6.** FTIR analyses of samples. (a) Full and (b,c) expanded range FTIR spectra of resveratrol powder, HP $\beta$ CD NF, resveratrol/HP $\beta$ CD NF, HP $\gamma$ CD NF, resveratrol/HP $\gamma$ CD NF, pullulan NF, and resveratrol/pullulan NF.

at 6.6, 16.4, 19.2, 22.4, 23.6, and 28.4°. It can also be observed that for the pristine nanofibrous films of HP $\beta$ CD, HP $\gamma$ CD, and pullulan, there are broad peaks corresponding to the amorphous structures of the samples. For the inclusion complex system, XRD finding can prove the interaction between CD and guest by the disappearance, shift, or attenuation of the characteristic peaks of guest molecules.<sup>34,54</sup> For resveratrol/HP $\gamma$ CD nanofibrous films, tiny crystalline peaks of resveratrol at 16.4 and 19.2° pointing to the remaining uncomplexed active compounds in the sample were detected. To contrast, these peaks were not observed in the resveratrol/HP $\beta$ CD nanofibrous film. A similar amorphous characteristic of the pristine HP $\beta$ CD was found in the case of nanofibrous film of resveratrol/HP $\beta$ CD suggesting the full encapsulation of the resveratrol molecules inside the HP $\beta$ CD cavities. Here, the resveratrol molecules were separated from each other and could not come together to form the crystals again, so the distinctive peaks of resveratrol were not detected in the XRD graph of the resveratrol/HP $\beta$ CD nanofibrous film. In the control sample of resveratrol/pullulan, the distinct peaks of resveratrol were detected at 6.6, 13.4, 16.4, 19.2, 22.4, and 25.4°, since there are no complex structures in this sample.

Here, thermal characterization of samples was conducted using the DSC technique which can also be utilized to clarify the interaction between CD and guest molecules by the shifts, broadenings, disappearances, or attenuation observed in the volatilization, melting, decomposition, or oxidation peaks of components.<sup>54,55</sup> In general, inclusion complexation raises absence, broadening, or intensity remission of the endothermic

peaks of guest molecules.<sup>54,55</sup> As presented in Figure S1a, the DSC curve of resveratrol displays a sharp endothermic peak at 266 °C corresponding to its melting point. On the other hand, the broad endothermic peak detected at around 90 °C for other samples corresponds to the water loss. The melting peak of resveratrol was not observed in the case of the resveratrol/CD nanofibrous film confirming that the guest molecule remained in an almost completely amorphous state in the samples. A small endothermic peak was observed for the resveratrol/pullulan nanofibrous film at around 240 °C differently from other resveratrol-incorporated samples which suggested the crystal state of resveratrol in the sample (Figure S1b). As another thermal behavior analysis, TGA was performed, and the results of the analysis are displayed in Figure S2. Here, resveratrol powder indicated weight loss which started at around 200 °C and ended up at 400 °C. The pristine- or resveratrol-included CD and pullulan nanofibrous films have primary weight loss up to 100 °C rising from the dehydration of the samples (Figure S2). The pristine CD and pullulan nanofibrous film exhibit, respectively, main weight loss in the ranges of 260–430 and 200–480 °C due to main thermal degradation (Figure S2). Principally, the inclusion complexation can improve the thermal stability of guest molecules. This might be detected by shifting of the thermal degradation step of guest to the higher temperatures.<sup>56</sup> In the case of the resveratrol/CD nanofibrous film, an additional degradation step was not observed for resveratrol, it was overlapped with the main degradation of CD suggesting the enhanced thermal stability of the guest molecule by the

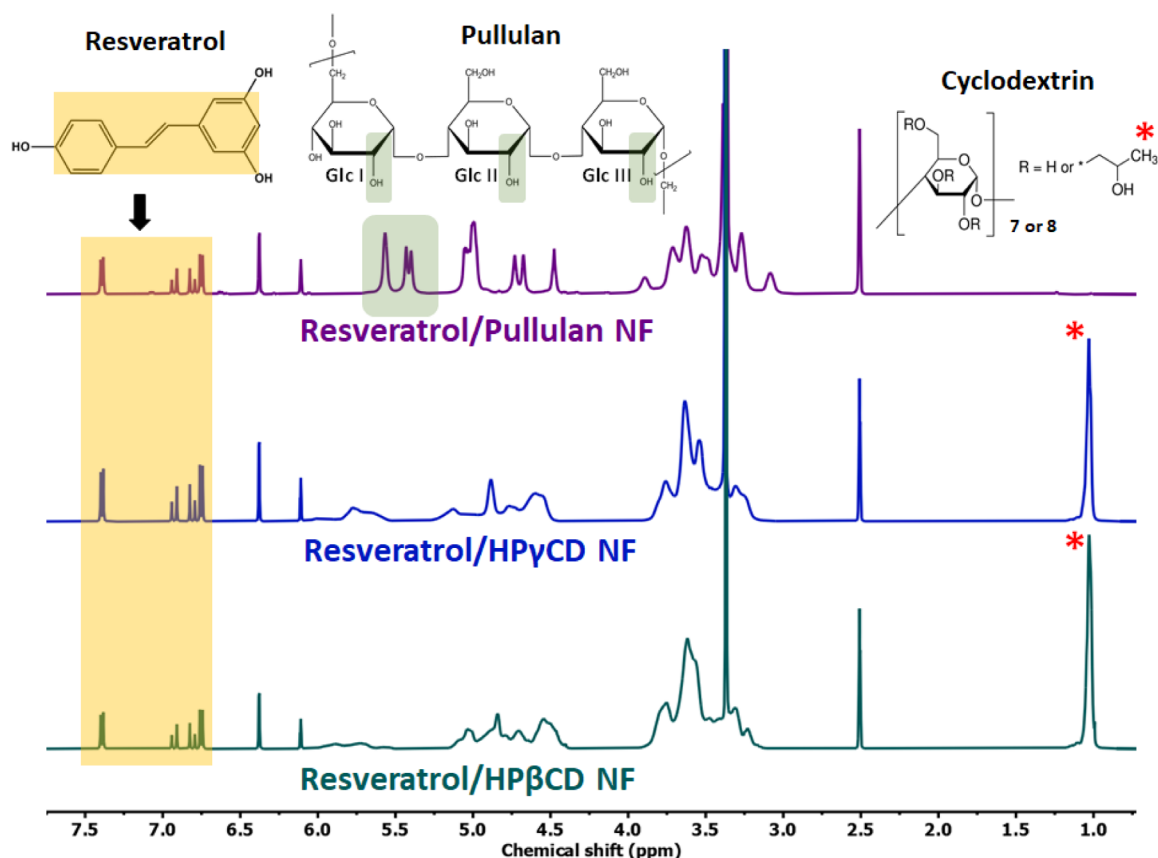


**Figure 7.** Chemical structure of samples.  $^1\text{H}$  NMR spectra of resveratrol/HP $\beta$ CD NF, resveratrol/HP $\gamma$ CD NF, and resveratrol/pullulan NF which were recorded by dissolving samples in  $\text{DMSO-}d_6$ .

formation of an interaction between CD and guest molecules (Figure S2 a,bii). On the other hand, the degradation step of resveratrol was detected for the resveratrol/pullulan nanofibrous film as an additional step at around 240 °C. Briefly, both DSC and TGA results validated the inclusion complex formation between resveratrol and CD. However, the uncomplex part of resveratrol could not be detected in the resveratrol/HP $\gamma$ CD nanofibrous film just like it was identified from XRD analysis (Figure 5) and the reason might be the different sensibilities of the techniques.

Figure 6 displays the FTIR spectra of resveratrol powder, CD, pullulan, resveratrol/CD, and resveratrol/pullulan nanofibrous films. FTIR is also a commonly used technique to examine the inclusion complex formation.<sup>54</sup> Attenuation, shift, or disappearance of the characteristic peaks of the components can be observed in the FTIR spectrum depending on the interaction between CD and guest molecules.<sup>54</sup> The major peaks of CD were identified at around 1020–1200  $\text{cm}^{-1}$  (coupled C–C/C–O and antisymmetric C–O–C stretching), 1370  $\text{cm}^{-1}$  (–CH<sub>3</sub> bending vibrations), 1650  $\text{cm}^{-1}$  (O–H bending), 2930  $\text{cm}^{-1}$  (C–H stretching), and 3000–3600  $\text{cm}^{-1}$  (primary/secondary –OH stretching).<sup>57</sup> Pullulan has analogous peaks in the parallel region with CD due to their similar chemical structures including  $\nu(\text{C–O})$  stretching at 1020–1200  $\text{cm}^{-1}$ ; H–O–H bending at 1641  $\text{cm}^{-1}$ ;  $\nu(\text{C–H})$  stretching at 2925  $\text{cm}^{-1}$ ; and  $\nu(\text{O–H})$  stretching at 3313  $\text{cm}^{-1}$ .<sup>58</sup> Pure resveratrol peaks of 1510  $\text{cm}^{-1}$  (benzene skeleton vibrations) and 1583  $\text{cm}^{-1}$  (C–C olefinic stretching) shifted, respectively, to 1590 and 1516  $\text{cm}^{-1}$  in the case of resveratrol/CD nanofibrous films. Additionally, the peaks of resveratrol at

828 and 804  $\text{cm}^{-1}$  corresponding to =C–H vibration shifted to 840 and 799  $\text{cm}^{-1}$ , respectively. The shifts which were also pointed in the expanded areas of FTIR graphs (Figure 6b,c) confirmed the inclusion complex formation between resveratrol and CD molecules.<sup>54</sup> For the resveratrol/pullulan nanofibrous film, the peaks of resveratrol at 828, 1510, and 1583  $\text{cm}^{-1}$  were observed without shift, and this observation proved the existence of the active compound in the absence of specific interaction with pullulan.

In this study, the initial molar ratio of 1:2 (resveratrol/CD) was used for the preparation of the resveratrol/CD inclusion complex aqueous system which corresponds to the ~7% (w/w) of resveratrol content in the nanofibrous film. Here,  $^1\text{H}$  NMR was used to determine the approximate loading capacity (% w/v) of electrospun samples. Figure 7 indicates the  $^1\text{H}$  NMR spectra of resveratrol/HP $\beta$ CD, resveratrol/HP $\gamma$ CD, and resveratrol/pullulan nanofibrous films which were recorded by dissolving samples in  $\text{DMSO-}d_6$  prior to the measurement. The integrated area of the characteristic peaks of resveratrol, CD, and pullulan, which are highlighted in Figure 7, was utilized for the calculations. The final molar ratio between CD and resveratrol in resveratrol/HP $\beta$ CD and resveratrol/HP $\gamma$ CD nanofibrous films was detected as ~1:2 (resveratrol/CD) [~7% (w/w)] showing the complete preservation of the active compound over the course of process. In the case of the resveratrol/pullulan nanofibrous film, the loading capacity was also determined as ~7% (w/w). It is also noteworthy to mention that the resveratrol has the identical characteristic peaks for electrospun samples suggesting its protected chemical structure during the electrospinning (Figure 7).



The further loading efficiency test was conducted by dissolving nanofibrous films in DMSO. Here, results were found to be compatible with the  $^1\text{H}$  NMR measurement such that the loading efficiency values of all samples were detected as  $\sim 100\%$  corresponding to the  $\sim 7\%$  (w/w) loading capacity. The statistical analysis also revealed that the means of the two CD types are not significantly different from each other ( $p > 0.05$ ). Briefly, the initial resveratrol content was protected for resveratrol/HP $\beta$ CD, resveratrol/HP $\gamma$ CD, and resveratrol/pullulan nanofibrous films, further confirming the total encapsulation of the resveratrol molecules.

**3.5. Dissolution and Disintegration Profiles.** The dissolution behavior of resveratrol/HP $\beta$ CD, resveratrol/HP $\gamma$ CD, and resveratrol/pullulan nanofibrous films was visually examined by adding water into the glass vials (Figure 8i and Video S1). For comparison, pristine resveratrol powder was analyzed, as well. As seen in the captured images in Figure 8ai, pristine resveratrol powder remained undissolved on the surface of the water for the entire profiling, proving its poor water solubility ( $\sim 0.17$  mM). Here, both resveratrol/CD nanofibrous films were able to complete total dissolution and form clear solutions in less than 2 s (Figure 8b-i,c-i), while there was still a remaining layer of undissolved sample in the vial upon 15 s in the case of the resveratrol/pullulan nanofibrous film (Figure 8d-i). The lower water solubility of the pullulan polymer ( $\sim 500$  mg/mL) compared to hydroxypropylated CD ( $>2000$  mg/mL) and the uncomplexed and crystal state of resveratrol in the resveratrol/pullulan nanofibrous film might lead to the worse dissolution profile than resveratrol/CD-based samples. Besides the extremely high aqueous solubility of HP $\beta$ CD and HP $\gamma$ CD, the amorphous distribution of resveratrol in these nanofibrous films also ensured an immediate dissolution upon contact with aqueous medium (Figure 8-i). It was discussed in the previous sections that there were detected uncomplexed parts of resveratrol in the resveratrol/HP $\gamma$ CD nanofibrous film. However, they were not obvious in the vial of sample used for the dissolution test since the crystal part had a small portion throughout the nanofibrous film.

Additionally, the disintegration behavior of resveratrol/CD and resveratrol/pullulan nanofibrous films was studied using the simulated environment of oral cavity.<sup>45</sup> Photographs captured from Video S2 are depicted in Figure 8ii. Here, resveratrol/CD nanofibrous films were immediately absorbed and disintegrated in less than 5 s upon contact with filter paper which was wetted with artificial saliva (Figure 8a-ii,b-ii). Even, there was crystalline state of resveratrol in the resveratrol/pullulan nanofibrous film, the sample was absorbed by the simulated environment in less than 5 s; however, a thin layer of film remained on the Petri dish (Figure 8c-ii). This might be initiated by the content of crystalline resveratrol and also lower aqueous solubility of pullulan compared to CD-based systems. The high water solubility of hydroxypropylated derivatives of HP $\beta$ CD and HP $\gamma$ CD was an influential dynamic for the fast disintegration of nanofibrous samples.<sup>59</sup> The high surface area and porous feature of nanofibrous films also guaranteed the penetration of water through the fibrous structure effectively and created active interaction sides for aqueous medium during both dissolution and disintegration processes.<sup>6</sup> Here, the inclusion complexation also ensured an enhanced solubility for resveratrol by the amorphization of the compound and this can enhance the bioavailability of resveratrol during its treatment.<sup>60</sup> To conclude, resveratrol/CD nanofibrous films

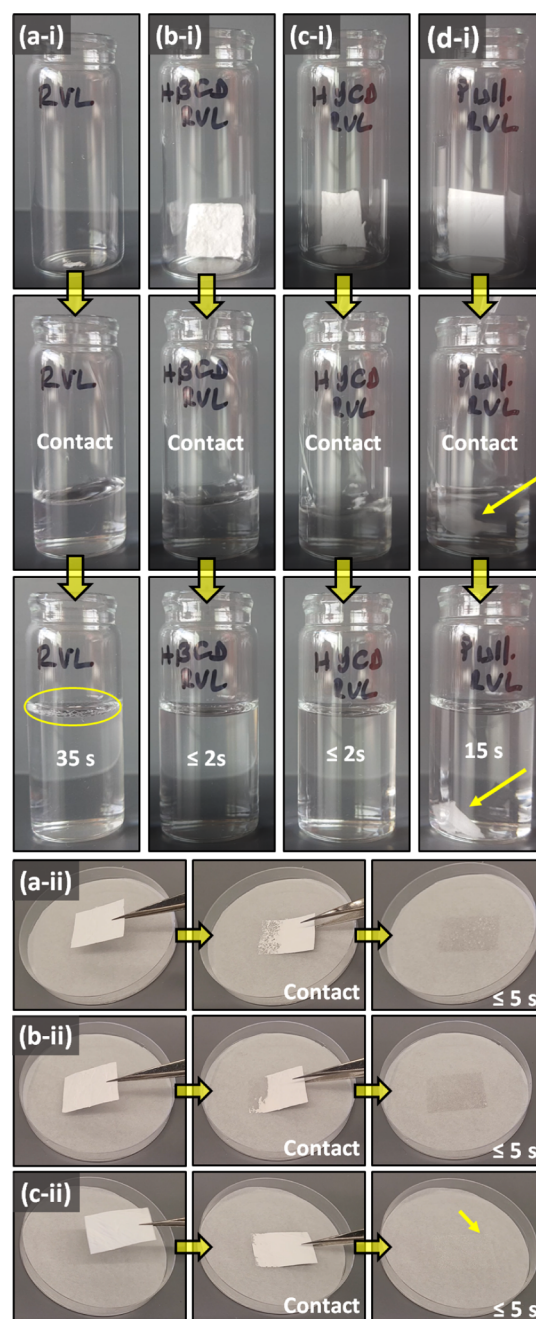


**Figure 8.** Dissolution and disintegration profiles of samples. Dissolution behavior of (a-i) resveratrol powder, (b-i) resveratrol/HP $\beta$ CD NF, (c-i) resveratrol/HP $\gamma$ CD NF, and (d-i) resveratrol/pullulan NF (The pictures are captured from Video S1). Disintegration behavior of (a-ii) resveratrol/HP $\beta$ CD NF, (b-ii) resveratrol/HP $\gamma$ CD NF, and (c-ii) resveratrol/pullulan NF (The pictures are captured from Video S2).

would be more suitable for an orally fast-disintegrating delivery system, as it would disintegrate rapidly and without leaving a grainy feeling behind upon administration.

**3.6. In Vitro Release Profile.** In this study, the time-dependent release profiles of resveratrol powder, resveratrol/HP $\beta$ CD, resveratrol/HP $\gamma$ CD, and resveratrol/pullulan nanofibrous films were examined in PBS buffer having pH 7.4 and the plotted graph is depicted in Figure 9a. As it is seen, resveratrol/HP $\beta$ CD and resveratrol/HP $\gamma$ CD nanofibrous films reached a high release concentration of  $85.0 \pm 7.6$  and  $78.9 \pm$

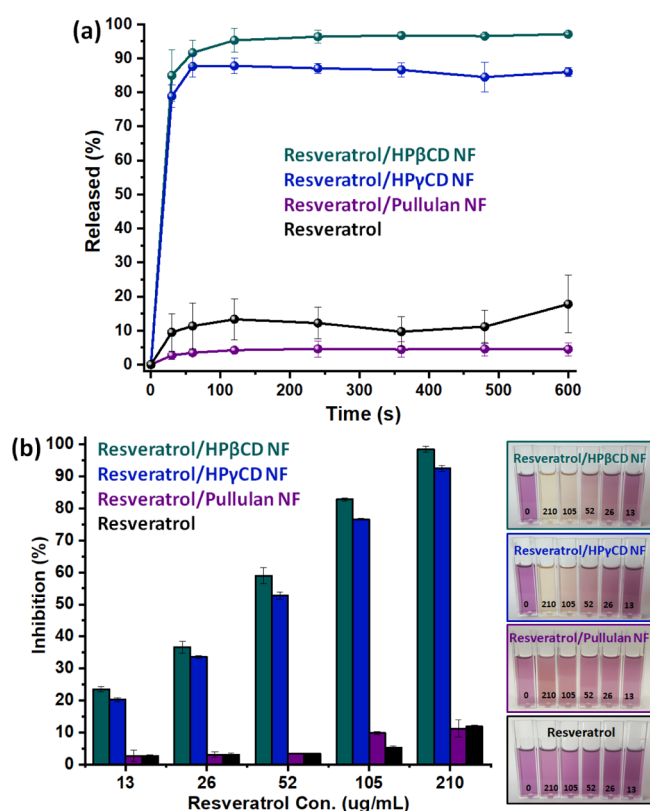


**Figure 9.** Release profile and antioxidant properties of samples. (a) Time-dependent release profiles of resveratrol powder, resveratrol/HPβCD NF, resveratrol/HPγCD NF, and resveratrol/pullulan NF. (b) Concentration-dependent antioxidant performance graphs and the representative solution photographs of resveratrol powder, resveratrol/HPβCD NF, resveratrol/HPγCD NF, and resveratrol/pullulan NF.

3.4%, respectively, just in 30 s. Then, almost plateau profile was monitored over 10 min with the highest release concentration of  $97.1 \pm 0.5$  and  $86.0 \pm 1.3\%$  for resveratrol/HPβCD and resveratrol/HPγCD nanofibrous films, respectively. The higher release profile of the resveratrol/HPβCD nanofibrous film compared to the resveratrol/HPγCD one increased from the trace quantities of resveratrol crystals existed in the HPγCD-based sample. On the other hand, resveratrol powder and resveratrol/pullulan nanofibrous film only reached the release concentration of  $9.4 \pm 5.4$  and  $2.7 \pm 1.2\%$ , respectively, in 30 s and released  $17.8 \pm 8.5$  and  $4.5 \pm 1.9\%$  of resveratrol at the end of 10 min (Figure 9a). The significant difference between samples was also confirmed by the statistical analysis ( $p < 0.05$ ). Here, the release of crystals occurred by the steady dissolution of resveratrol molecules in the aqueous medium, so it highly depended on the intrinsic solubility of resveratrol in water ( $\sim 0.17$  mM). Since resveratrol crystals were encapsulated in an additional polymeric matrix in the case of the resveratrol/pullulan nanofibrous film, it might have created a barrier for the resveratrol molecules during exuding into the liquid medium, so the lower and slower release was detected for nanofiber-based samples compared to the powder form of active compound (Figure 9a). These findings revealed that inclusion complexation ensured an enhanced solubility and so higher release profile for resveratrol compared to its pristine powder form or crystal form encapsulated into another type of polymeric matrix. Besides the amorphous state of resveratrol in

the case of inclusion complexes, the significantly higher aqueous solubility of HPβCD and HPγCD ( $>2000$  mg/mL) compared to pullulan ( $\sim 500$  mg/mL) might also lead to a much better release profile for CD-based samples by the faster dissolution in the liquid medium.

In order to examine the release profiles, different kinetic models were applied further, and the formulations and the  $R^2$  (regression coefficient) values are given in the Supporting Information (Table S2). The results revealed that the release profile of samples fits with the neither zero/first-order kinetics nor the Higuchi model and this confirmed that the release of resveratrol did not happen in a time-dependent manner from an insoluble planar matrix in water (Fick's first law).<sup>61</sup> On the other hand, relatively higher coherence was detected with the Korsmeyer–Peppas model compared to others and this finding established the erosion and diffusion-controlled release of resveratrol. The slope of the fitted graphs of Korsmeyer–Peppas equations enables to calculate the diffusion exponent ( $n$ ) value.<sup>61,62</sup> For CD inclusion complex nanofibrous films, the  $n$  value was found in the range of  $0.45 < n < 0.89$  pointing to the non-Fickian or anomalous diffusion of resveratrol from samples. In the case of the resveratrol/pullulan nanofibrous film and resveratrol powder, the quasi-Fickian diffusion profile was determined with  $n < 0.45$  value (Table S2).<sup>63</sup>

**3.7. Antioxidant Activity Profile.** Reactive oxygen species (ROS) or free radical can lead to cancer, stroke, and neurodegenerative diseases as a result of oxidation of various biomolecules including DNA, proteins, and lipids.<sup>64</sup> Antioxidant agents can hinder the destructive consequences of free radicals and ROS by inhibiting them.<sup>64</sup> Resveratrol is a well-known phenolic compound which indicates antioxidant activity by donating the hydrogen atom from its phenol group to the radical acceptor.<sup>65</sup> Here, the DPPH assay was used to examine the antioxidant property of samples and the reduction at the absorbance intensity of DPPH (517 nm) was followed for the analysis. In this study, antioxidant performance of samples was investigated for the different concentrations of resveratrol (13–210 μg/mL) encapsulated in the nanofibrous films. For control, the powder form of resveratrol was also evaluated for the same concentration range. Figure 9b shows the radical inhibition (%) graphs of samples against the increasing concentration of resveratrol with the representative photographs of the antioxidant test solutions. As it was expected, higher scavenging activity was obtained for the higher concentration of resveratrol (Figure 9b). For the highest resveratrol concentration (210 μg/mL), resveratrol/HPβCD and resveratrol/HPγCD nanofibrous films displayed  $98.5 \pm 0.9$  and  $92.6 \pm 0.9\%$  radical scavenging performance, respectively. On the other hand, resveratrol powder and resveratrol/pullulan nanofibrous film indicated uttermost  $11.9 \pm 0.5$  and  $11.2 \pm 2.6\%$  inhibition activity, respectively, in the given concentration range. These findings are also correlated with the photographs of DPPH systems where the color of solutions of resveratrol/CD nanofibrous films became yellow, while the color of control sample solutions (resveratrol and resveratrol/pullulan) remained purple hue (Figure 9b). As it was addressed in the previous parts, there was a trace amount of uncomplexed, so the crystal resveratrol part in the resveratrol/HPγCD nanofibrous film and this might lead to slightly lower radical scavenging compared to the resveratrol/HPβCD nanofibrous film. The significantly better antioxidant potential of the resveratrol/CD nanofibrous film compared to control samples is due to the amorphous state and the enhanced



aqueous solubility of resveratrol by inclusion complexation such that a higher amount of resveratrol took part in the radical scavenging process. It is noteworthy to mention that the pristine CD and pullulan nanofibrous films did not show a radical inhibition activity (data are not given). The concentration-dependent antioxidant test enabled to calculate the IC<sub>50</sub> value of samples which corresponds to the concentration of the active compound needed to scavenge the 50% of initial DPPH concentration.<sup>46</sup> The IC<sub>50</sub> value of resveratrol/HP $\beta$ CD, resveratrol/HP $\gamma$ CD, resveratrol/pullulan nanofibrous films, and resveratrol powder was determined to be 41.7, 47.8, 1056.2, and 901.6  $\mu$ g/mL, respectively. In other words, less amount of substrate is needed in the case of resveratrol/CD-based samples compared to the resveratrol/pullulan nanofibrous film and resveratrol powder to obtain an antioxidant property. The significant difference between samples were also confirmed by the statistical analysis ( $p < 0.05$ ).

To conclude, the inclusion complex nanofibrous films of resveratrol were generated using two different derivatives of CD (HP $\beta$ CD and HP $\gamma$ CD) without using a carrier polymeric matrix. The free-standing, flexible, and foldable nanofibrous films were obtained with homogeneous and defect-free morphology for both CD types using the molar ratio of 1:2 (guest/CD). The polymeric resveratrol/pullulan nanofibrous film was also produced as the control sample. The loading efficiency of nanofibrous films was determined to be  $\sim$ 7% (w/w, with respect to the final sample) and this revealed that all samples were obtained having  $\sim$ 100% loading efficiency without a loss during the process. While phase solubility findings indicated that HP $\beta$ CD can form more favorable inclusion complexes with resveratrol compared to HP $\gamma$ CD, computational modeling study showed that 1:2 molar ratio is energetically more preferred compared to 1:1. The amorphization of resveratrol crystals as a result of inclusion complexation was verified using XRD and DSC techniques. The inclusion complex formation was further proved by FTIR measurements. <sup>1</sup>H NMR findings revealed that the chemical structure of resveratrol was preserved along the whole procedure comprising the preparation of solutions and electrospinning process. The solubility of the poorly water-soluble resveratrol was significantly enhanced in the case of CD-based nanofibrous films such that resveratrol/CD nanofibrous films showed a faster release/dissolution profile in liquid medium compared to the polymeric system of pullulan by releasing  $\sim$ 79–85% of resveratrol just in 30 s. Moreover, resveratrol/CD nanofibrous films were immediately absorbed by the saliva simulation and disintegrated in less than 5 s upon contact while the thin layer of the resveratrol/pullulan nanofibrous film remained on the filter paper after the absorption by artificial saliva. Additionally, the antioxidant efficiency of resveratrol was significantly improved for resveratrol/CD nanofibrous films as a result of its improved aqueous solubility. Here, higher water solubility, better release and antioxidant profiles were attained for the HP $\beta$ CD-based nanofibrous film compared to the HP $\gamma$ CD one due to more favorable complex formation between HP $\beta$ CD and resveratrol. Here, polymer-free resveratrol/CD nanofibrous films were generated using water in the absence of supplementary toxic solvents or chemicals. This is particularly attractive for the food- and pharmaceutical-based applications and is important for the industrialization of CD inclusion complex nanofibrous films. Briefly, the unique properties of CD inclusion complexes and electrospun

nanofibrous films were integrated for developing a new-generation dietary supplement formulation having orally fast-disintegrating feature. This innovative design can be considered as a promising step in the development of an alternative route of resveratrol administration and can pave the way of avoiding metabolic instability of this bioactive compound by employing fast disintegration in the oral mucosa.

## ■ ASSOCIATED CONTENT

### SI Supporting Information

The Supporting Information is available free of charge at <https://pubs.acs.org/doi/10.1021/acsfoodscitech.1c00456>.

Solution properties (viscosity and conductivity) and the fiber diameters of resulting electrospun nanofibers; full and expanded DSC thermograms of samples; TGA thermograms/derivatives of samples; mathematical models for release kinetics; results ( $R^2$ ) of release kinetics calculations (PDF)

Video S1: Dissolution behavior of samples (MP4)

Video S2: Disintegration behavior of samples (MP4)

## ■ AUTHOR INFORMATION

### Corresponding Authors

Asli Celebioglu – Fiber Science Program, Department of Human Centered Design College of Human Ecology, Cornell University, Ithaca, New York 14853, United States; [orcid.org/0000-0002-5563-5746](https://orcid.org/0000-0002-5563-5746); Email: [tu46@cornell.edu](mailto:tu46@cornell.edu)

Tamer Uyar – Fiber Science Program, Department of Human Centered Design College of Human Ecology, Cornell University, Ithaca, New York 14853, United States; [orcid.org/0000-0002-3989-4481](https://orcid.org/0000-0002-3989-4481); Email: [ac2873@cornell.edu](mailto:ac2873@cornell.edu)

### Authors

Deniz Tekant – Operations Research and Information Engineering, College of Engineering, Cornell University, Ithaca, New York 14853, United States

Mehmet Emin Kilic – Computational Science Research Center, Korea Institute of Science and Technology, Seoul 02792, Republic of Korea; [orcid.org/0000-0003-1814-5104](https://orcid.org/0000-0003-1814-5104)

Engin Durgun – UNAM-National Nanotechnology Research Center and Institute of Materials Science and Nanotechnology, Bilkent University, Ankara 06800, Turkey; [orcid.org/0000-0002-0639-5862](https://orcid.org/0000-0002-0639-5862)

Complete contact information is available at: <https://pubs.acs.org/10.1021/acsfoodscitech.1c00456>

### Author Contributions

<sup>†</sup>A.C. and D.T. contributed equally.

### Author Contributions

A.C. performed conceptualization, methodology, investigation, and writing of the original draft. D.T. performed investigation and writing of the original draft. M.E.K. and E.D. participated in investigation and writing of the computational modeling study. T.U. supervised the study and participated in conceptualization, methodology, editing the final version, funding acquisition, and project administration of the study.

### Notes

The authors declare no competing financial interest.



## ACKNOWLEDGMENTS

This work made use of the Cornell Center for Materials Research Shared Facilities which are supported through the NSF MRSEC program (DMR-1719875), the Cornell Chemistry NMR Facility supported in part by the NSF MRI program (CHE-1531632), and Department of Human Centered Design facilities. M.E.K. acknowledges support from Brain Pool Program through the National Research Foundation of Korea (NRF) funded by the Ministry of Science and ICT (2020H1D3A1A02081517).

## REFERENCES

- (1) Hosseini, H.; Jafari, S. M. Introducing Nano/Microencapsulated Bioactive Ingredients for Extending the Shelf-Life of Food Products. *Adv. Colloid Interface Sci.* **2020**, *282*, 102210.
- (2) Munteanu, B. S.; Vasile, C. Encapsulation of Natural Bioactive Compounds by Electrospinning—Applications in Food Storage and Safety. *Polymers* **2021**, *13*, 3771.
- (3) Leidy, R.; Maria Ximena, Q.-C. Use of Electrospinning Technique to Produce Nanofibres for Food Industries: A Perspective from Regulations to Characterisations. *Trends Food Sci. Technol.* **2019**, *85*, 92–106.
- (4) Xue, J.; Wu, T.; Dai, Y.; Xia, Y. Electrospinning and Electrospun Nanofibers: Methods, Materials, and Applications. *Chem. Rev.* **2019**, *119*, 5298–5415.
- (5) Torres-Giner, S.; Busolo, M.; Cherpinski, A.; Lagaron, J. M. Electrospinning in the Packaging Industry. *Electrospinning*; The Royal Society of Chemistry, 2018; pp 238–260.
- (6) Yu, D.-G.; Li, J.-J.; Williams, G. R.; Zhao, M. Electrospun Amorphous Solid Dispersions of Poorly Water-Soluble Drugs: A Review. *J. Controlled Release* **2018**, *292*, 91–110.
- (7) Balusamy, B.; Celebioglu, A.; Senthamizhan, A.; Uyar, T. Progress in the Design and Development of “Fast-Dissolving” Electrospun Nanofibers Based Drug Delivery Systems - A Systematic Review. *J. Controlled Release* **2020**, *326*, 482–509.
- (8) Celebioglu, A.; Uyar, T. Fast-Dissolving Antioxidant Curcumin/Cyclodextrin Inclusion Complex Electrospun Nanofibrous Webs. *Food Chem.* **2020**, *317*, 126397.
- (9) Celebioglu, A.; Uyar, T. Development of Ferulic Acid/Cyclodextrin Inclusion Complex Nanofibers for Fast-Dissolving Drug Delivery System. *Int. J. Pharm.* **2020**, *584*, 119395.
- (10) Celebioglu, A.; Uyar, T. Encapsulation and Stabilization of  $\alpha$ -Lipoic Acid in Cyclodextrin Inclusion Complex Electrospun Nanofibers: Antioxidant and Fast-Dissolving  $\alpha$ -Lipoic Acid/Cyclodextrin Nanofibrous Webs. *J. Agric. Food Chem.* **2019**, *67*, 13093–13107.
- (11) Bilensoy, E. *Cyclodextrins in Pharmaceuticals, Cosmetics, and Biomedicine: Current and Future Industrial Applications*; John Wiley Sons, 2011.
- (12) Carneiro, S.; Costa Duarte, F.; Heimfarth, L.; Siqueira Quintans, J.; Quintans-Júnior, L.; Veiga Júnior, V.; Neves de Lima, A.; Veiga Júnior, V. F. d.; Neves de Lima, A. A. Cyclodextrin–Drug Inclusion Complexes: In Vivo and In Vitro Approaches. *Int. J. Mol. Sci.* **2019**, *20*, 642.
- (13) Crini, G. History of Cyclodextrins. *Chem. Rev.* **2014**, *114*, 10940–10975.
- (14) GRAS Notice of Cyclodextrin (GRN No. 678, 74, 46) 2022. [https://www.cfsanappsexternal.fda.gov/scripts/fdcc/?set=GRASNotices&sort=GRN\\_No&order=DESC&startrow=1&type=basic&search=cyclodextrin](https://www.cfsanappsexternal.fda.gov/scripts/fdcc/?set=GRASNotices&sort=GRN_No&order=DESC&startrow=1&type=basic&search=cyclodextrin).
- (15) Marques, H. M. C. A Review on Cyclodextrin Encapsulation of Essential Oils and Volatiles. *Flavour Fragrance J.* **2010**, *25*, 313–326.
- (16) Kalepu, S.; Nekkanti, V. Insoluble Drug Delivery Strategies: Review of Recent Advances and Business Prospects. *Acta Pharm. Sin. B* **2015**, *5*, 442–453.
- (17) Seethu, B. G.; Pushpadass, H. A.; Emerald, F. M. E.; Nath, B. S.; Naik, N. L.; Subramanian, K. S. Electrohydrodynamic Encapsulation of Resveratrol Using Food-Grade Nanofibers: Process Optimization, Characterization and Fortification. *Food Bioprocess Technol.* **2020**, *13*, 341–354.
- (18) Li, L.; Wang, H.; Chen, M.; Jiang, S.; Cheng, J.; Li, X.; Zhang, M.; Jiang, S. Gelatin/Zein Fiber Mats Encapsulated with Resveratrol: Kinetics, Antibacterial Activity and Application for Pork Preservation. *Food Hydrocolloids* **2020**, *101*, 105577.
- (19) Lin, Y.-C.; Hu, S. C.-S.; Huang, P.-H.; Lin, T.-C.; Yen, F.-L. Electrospun Resveratrol-Loaded Polyvinylpyrrolidone/Cyclodextrin Nanofibers and Their Biomedical Applications. *Pharmaceutics* **2020**, *12*, 552.
- (20) Amri, A.; Chaumeil, J. C.; Sfar, S.; Charrueau, C. Administration of Resveratrol: What Formulation Solutions to Bioavailability Limitations? *J. Controlled Release* **2012**, *158*, 182–193.
- (21) Davidov-Pardo, G.; McClements, D. J. Resveratrol Encapsulation: Designing Delivery Systems to Overcome Solubility, Stability and Bioavailability Issues. *Trends Food Sci. Technol.* **2014**, *38*, 88–103.
- (22) Santos, A. C.; Pereira, L.; Pereira-Silva, M.; Ferreira, L.; Caldas, M.; Collado-González, M.; Magalhães, M.; Figueiras, A.; Ribeiro, A. J.; Veiga, F. Nanotechnology-Based Formulations for Resveratrol Delivery: Effects on Resveratrol in Vivo Bioavailability and Bioactivity. *Colloids Surf., B* **2019**, *180*, 127–140.
- (23) Karimi-Soflou, R.; Mohseni-Vadeghani, E.; Karkhaneh, A. Controlled Release of Resveratrol from a Composite Nanofibrous Scaffold: Effect of Resveratrol on Antioxidant Activity and Osteogenic Differentiation. *J. Biomed. Mater. Res., Part A* **2022**, *110*, 21–30.
- (24) Ma, W.; Zhou, M.; Dong, W.; Zhao, S.; Wang, Y.; Yao, J.; Liu, Z.; Han, H.; Sun, D.; Zhang, M. A Bi-Layered Scaffold of a Poly (Lactic-Co-Glycolic Acid) Nanofiber Mat and an Alginate–Gelatin Hydrogel for Wound Healing. *J. Mater. Chem. B* **2021**, *9*, 7492–7505.
- (25) Bonadies, I.; Di Cristo, F.; Valentino, A.; Peluso, G.; Calarco, A.; Di Salle, A. PH-Responsive Resveratrol-Loaded Electrospun Membranes for the Prevention of Implant-Associated Infections. *Nanomaterials* **2020**, *10*, 1175.
- (26) Maria Leena, M.; Yoha, K. S.; Moses, J. A.; Anandharamkrishnan, C. Edible Coating with Resveratrol Loaded Electrospun Zein Nanofibers with Enhanced Bioaccessibility. *Food Biosci.* **2020**, *36*, 100669.
- (27) Rahane, R.; Rachh, P. R. A Review on Fast Dissolving Tablet. *J. Drug Delivery Ther.* **2018**, *8*, 50–55.
- (28) Patil, P. C.; Shrivastava, S. K.; Vaidehi, S.; Ashwini, P. Oral Fast Dissolving Drug Delivery System: A Modern Approach for Patient Compliance. *Int. J. Drug Regul. Aff.* **2014**, *2*, 49–60.
- (29) Chimento, A.; De Amicis, F.; Sirianni, R.; Sinicropi, M.; Puoci, F.; Casaburi, I.; Saturnino, C.; Pezzi, V. Progress to Improve Oral Bioavailability and Beneficial Effects of Resveratrol. *Int. J. Mol. Sci.* **2019**, *20*, 1381.
- (30) Di Prima, G.; Angellotti, G.; Scarpaci, A. G.; Murgia, D.; D’agostino, F.; Campisi, G.; De Caro, V. Improvement of Resveratrol Permeation through Sublingual Mucosa: Chemical Permeation Enhancers versus Spray Drying Technique to Obtain Fast-Disintegrating Sublingual Mini-Tablets. *Pharmaceutics* **2021**, *13*, 1370.
- (31) Paczkowska-Walendowska, M.; Dvořák, J.; Rosiak, N.; Tykarska, E.; Szymańska, E.; Winnicka, K.; Ruchala, M. A.; Cielecka-Piontek, J. Buccal Resveratrol Delivery System as a Potential New Concept for the Periodontitis Treatment. *Pharmaceutics* **2021**, *13*, 417.
- (32) De Vries, K.; Strydom, M.; Steenkamp, V. Bioavailability of Resveratrol: Possibilities for Enhancement. *J. Herb. Med.* **2018**, *11*, 71–77.
- (33) Celebioglu, A.; Uyar, T. Fast Dissolving Oral Drug Delivery System Based on Electrospun Nanofibrous Webs of Cyclodextrin/Ibuprofen Inclusion Complex Nanofibers. *Mol. Pharm.* **2019**, *16*, 4387–4398.
- (34) Celebioglu, A.; Uyar, T. Hydrocortisone/Cyclodextrin Complex Electrospun Nanofibers for a Fast-Dissolving Oral Drug Delivery System. *RSC Med. Chem.* **2020**, *11*, 245–258.
- (35) Celebioglu, A.; Uyar, T. Metronidazole/Hydroxypropyl- $\beta$ -Cyclodextrin Inclusion Complex Nanofibrous Webs as Fast-

- Dissolving Oral Drug Delivery System. *Int. J. Pharm.* **2019**, *572*, 118828.
- (36) Celebioglu, A.; Uyar, T. Electrospun Formulation of Acyclovir/Cyclodextrin Nanofibers for Fast-Dissolving Antiviral Drug Delivery. *Mater. Sci. Eng., C* **2021**, *118*, 111514.
- (37) Higuchi, T.; Connors, K. A. Phase Solubility Diagram. *Adv. Anal. Chem. Instrum.* **1965**, *4*, 117–212.
- (38) Kohn, W.; Sham, L. J. Self-Consistent Equations Including Exchange and Correlation Effects. *Phys. Rev.* **1965**, *140*, A1133.
- (39) Hohenberg, P.; Kohn, W. Inhomogeneous Electron Gas. *Phys. Rev.* **1964**, *136*, B864.
- (40) Kresse, G.; Furthmüller, J. Efficient Iterative Schemes for Ab Initio Total-Energy Calculations Using a Plane-Wave Basis Set. *Phys. Rev. B: Condens. Matter Mater. Phys.* **1996**, *54*, 11169.
- (41) Perdew, J. P.; Burke, K.; Ernzerhof, M. Generalized Gradient Approximation Made Simple. *Phys. Rev. Lett.* **1997**, *78*, 1396.
- (42) Grimme, S. Semiempirical GGA-type Density Functional Constructed with a Long-range Dispersion Correction. *J. Comput. Chem.* **2006**, *27*, 1787–1799.
- (43) Blöchl, P. E. Projector Augmented-Wave Method. *Phys. Rev. B: Condens. Matter Mater. Phys.* **1994**, *50*, 17953.
- (44) Mathew, K.; Sundararaman, R.; Letchworth-Weaver, K.; Arias, T. A.; Hennig, R. G. Implicit Solvation Model for Density-Functional Study of Nanocrystal Surfaces and Reaction Pathways. *J. Chem. Phys.* **2014**, *140*, 084106.
- (45) Bi, Y.; Sunada, H.; Yonezawa, Y.; Danjo, K.; Otsuka, A.; IIDA, K. Preparation and Evaluation of a Compressed Tablet Rapidly Disintegrating in the Oral Cavity. *Chem. Pharm. Bull.* **1996**, *44*, 2121–2127.
- (46) Ak, T.; Gülçin, İ. Antioxidant and Radical Scavenging Properties of Curcumin. *Chem.-Biol. Interact.* **2008**, *174*, 27–37.
- (47) Szente, L.; Fenyvesi, É. Cyclodextrin-Lipid Complexes: Cavity Size Matters. *Struct. Chem.* **2017**, *28*, 479–492.
- (48) Lu, Z.; Cheng, B.; Hu, Y.; Zhang, Y.; Zou, G. Complexation of Resveratrol with Cyclodextrins: Solubility and Antioxidant Activity. *Food Chem.* **2009**, *113*, 17–20.
- (49) Zhou, R.; Wang, F.; Guo, Z.; Zhao, Y. L. Preparation and Characterization of Resveratrol/Hydroxypropyl- $\beta$ -cyclodextrin Inclusion Complex Using Supercritical Antisolvent Technology. *J. Food Process Eng.* **2012**, *35*, 677–686.
- (50) Yang, Z.; Argenziano, M.; Salamone, P.; Pirro, E.; Sprio, A. E.; Di Scipio, F.; Carere, M. E.; Quaglino, E.; Cavallo, F.; Cavalli, R.; Berta, G. N. Preclinical Pharmacokinetics Comparison between Resveratrol 2-Hydroxypropyl- $\beta$ -Cyclodextrin Complex and Resveratrol Suspension after Oral Administration. *J. Inclusion Phenom. Macrocyclic Chem.* **2016**, *86*, 263–271.
- (51) Loftsson, T.; Frikdriksdóttir, H.; Sigurdardóttir, A. M.; Ueda, H. The Effect of Water-Soluble Polymers on Drug-Cyclodextrin Complexation. *Int. J. Pharm.* **1994**, *110*, 169–177.
- (52) Suvitha, A.; Venkataraman, N. S.; Sahara, R.; Kawazoe, Y. A Theoretical Exploration of the Intermolecular Interactions between Resveratrol and Water: A DFT and AIM Analysis. *J. Mol. Model.* **2019**, *25*, S6.
- (53) Uyar, T.; Besenbacher, F. Electrospinning of Uniform Polystyrene Fibers: The Effect of Solvent Conductivity. *Polymer* **2008**, *49*, 5336–5343.
- (54) Mura, P. Analytical Techniques for Characterization of Cyclodextrin Complexes in the Solid State: A Review. *J. Pharm. Biomed. Anal.* **2015**, *113*, 226–238.
- (55) Hädärugá, N. G.; Bandur, G. N.; David, I.; Hädärugá, D. I. A Review on Thermal Analyses of Cyclodextrins and Cyclodextrin Complexes. *Environ. Chem. Lett.* **2019**, *17*, 349–373.
- (56) Narayanan, G.; Boy, R.; Gupta, B. S.; Tonelli, A. E. Analytical Techniques for Characterizing Cyclodextrins and Their Inclusion Complexes with Large and Small Molecular Weight Guest Molecules. *Polym. Test.* **2017**, *62*, 402–439.
- (57) Yuan, C.; Liu, B.; Liu, H. Characterization of Hydroxypropyl- $\beta$ -Cyclodextrins with Different Substitution Patterns via FTIR, GC–MS, and TG–DTA. *Carbohydr. Polym.* **2015**, *118*, 36–40.

(58) Shao, P.; Niu, B.; Chen, H.; Sun, P. Fabrication and Characterization of Tea Polyphenols Loaded Pullulan-CMC Electrospun Nanofiber for Fruit Preservation. *Int. J. Biol. Macromol.* **2018**, *107*, 1908–1914.

(59) Loftsson, T.; Brewster, M. E. Pharmaceutical Applications of Cyclodextrins: Basic Science and Product Development. *J. Pharm. Pharmacol.* **2010**, *62*, 1607–1621.

(60) Preis, M. Orally Disintegrating Films and Mini-Tablets—Innovative Dosage Forms of Choice for Pediatric Use. *AAPS PharmSciTech* **2015**, *16*, 234–241.

(61) Peppas, N. A.; Narasimhan, B. Mathematical Models in Drug Delivery: How Modeling Has Shaped the Way We Design New Drug Delivery Systems. *J. Controlled Release* **2014**, *190*, 75–81.

(62) Li, X.; Kanjwal, M. A.; Lin, L.; Chronakis, I. S. Electrospun Polyvinyl-Alcohol Nanofibers as Oral Fast-Dissolving Delivery System of Caffeine and Riboflavin. *Colloids Surf., B* **2013**, *103*, 182–188.

(63) Akpan, U. M.; Pellegrini, M.; Obayemi, J. D.; Ezenwafor, T.; Browl, D.; Ani, C. J.; Yiporo, D.; Salifu, A.; Dozie-Nwachukwu, S.; Odusanya, S.; Freeman, J.; Soboyejo, W. O. Prodigiosin-Loaded Electrospun Nanofibers Scaffold for Localized Treatment of Triple Negative Breast Cancer. *Mater. Sci. Eng., C* **2020**, *114*, 110976.

(64) Gülçin, İ. Antioxidant Activity of Food Constituents: An Overview. *Arch. Toxicol.* **2012**, *86*, 345–391.

(65) Lucas-Abellán, C.; Mercader-Ros, M. T.; Zafrilla, M. P.; Gabaldón, J. A.; Núñez-Delgado, E. Comparative Study of Different Methods to Measure Antioxidant Activity of Resveratrol in the Presence of Cyclodextrins. *Food Chem. Toxicol.* **2011**, *49*, 1255–1260.

## Recommended by ACS

### Topical Application of 4'-Hydroxychalcone in Combination with *tt*-Farnesol Is Effective against *Candida albicans* and *Streptococcus mutans* Biofilms

Carmélia I. Lobo, Marlise I. Klein, *et al.*

JUNE 22, 2022  
ACS OMEGA

READ 

### Hydrolytic Quinoa Protein and Cationic Lotus Root Starch-Based Micelles for Co-Delivery of Quercetin and Epigallocatechin 3-Gallate in Ulcerative Colitis Treatment

Kang Liu, Xue-Qiang Zha, *et al.*

NOVEMBER 28, 2022  
JOURNAL OF AGRICULTURAL AND FOOD CHEMISTRY

READ 

### Orally Fast Disintegrating Cyclodextrin/Prednisolone Inclusion-Complex Nanofibrous Webs for Potential Steroid Medications

Asli Celebioglu, Tamer Uyar, *et al.*

NOVEMBER 15, 2021  
MOLECULAR PHARMACEUTICS

READ 

### Preparation, Characterization, and Evaluation of Curcumin–Graphene Oxide Complex-Loaded Liposomes against *Staphylococcus aureus* in Topical Disease

Mahfoozur Rahman, Sarwar Beg, *et al.*

NOVEMBER 20, 2022  
ACS OMEGA

READ 

Get More Suggestions >